



Non-lubricated dry sliding wear behavior of spark plasma sintered nano-structured stainless steel

R. Shashanka

Department of Metallurgical and Materials Engineering, Bartin University, Bartin-74100, Turkey

Received 20 Aug 2019,
Revised 26 Aug 2019,
Accepted 27 Aug 2019

Keywords

- ✓ Spark plasma sintering,
- ✓ Nano-structured stainless steel
- ✓ Wear,
- ✓ Wear mechanism,
- ✓ Wear debris

shashankaic@gmail.com;
Phone: +90 5415376803

Abstract

In the present paper we reported the non-lubricated sliding wear behavior of duplex and ferritic stainless steel against a diamond indenter. The ball milled nano-structured stainless steel powders were consolidated by spark plasma sintering technique at 1050°C. It has been found that spark plasma sintering (SPS) enhances the density, hardness and wear resistance of both the stainless steels. Maximum sintered density and Vickers microhardness is reported for duplex stainless steel than ferritic stainless steel. The wear studies of both the stainless steel were carried out using a pin-on-disc apparatus at 40 and 60 N against a diamond indenter. The wear mechanisms were found to be mainly abrasive and oxidative with mainly ploughing and plastic deformation modes. Semi-quantitative analysis of the worn out surfaces and wear debris were carried out using EDS to confirm the occurrence of oxidation processes during wear. The spark plasma sintered duplex stainless steel was found to exhibit maximum hardness and wear resistance than the spark plasma sintered ferritic stainless steel

1. Introduction

Stainless steel is one of the very important and popular materials in the world; used in different sectors like construction, marine, defence, automobiles, power plants etc. Different grades of stainless steels are there; but among them duplex and ferritic stainless steels are more significant. Duplex stainless steel is very important grade of stainless steel contains of almost equal ratios of austenite and ferrite phases [1]. The amalgamated effect of the two phases bestow good weldability, corrosion and wear resistance, high mechanical and creep strength, low thermal expansion, high temperature tensile strength etc. [2, 3]. Hence, duplex stainless steel is majorly used in de-salination plants, storage tanks, heat exchangers, paper and pulp industries, construction of bridges, flue gas cleaning, nuclear and chemical industries, structural design components, pressure vessels, impellers and shafts [4-6]. Whereas, ferritic stainless steels are another type of stainless steels bearing BCC structure and showcases the properties like high thermal conductivity, excellent corrosion resistance, creep resistance, high yield strength, magnetic property and high temperature oxidation resistance [7]. Due to these properties ferritic stainless steels are mainly used in cold water tanks, electric cabinets, water treatment plants, surgical instruments, refrigeration cabinets and other metallic implements [8-12]. Duplex and ferritic stainless steel can also be used as an electrochemical sensor in detecting various bioactive molecules such as dopamine, ascorbic acid and folic acid [3, 4, 13]. The above properties of both the stainless steel can be further amended by bringing down their structure to nano level (< 100 nm) or ultrafine level (100 to 1,000 nm) [14, 15]. The structure of stainless steel can be refined by using mechanical alloying method. Therefore, we had prepared nano-structured duplex and ferritic stainless steel powders by milling elemental Fe, Cr and Ni powders for 10 h in a dual drive planetary mill (DDPM). The detailed preparation of duplex and ferritic stainless steel, mill design and milling parameters were reported by the authors in their previous publications [8, 9, 16]. In the present paper, we are reporting the consolidation of 10 h ball milled duplex and ferritic stainless steel powders by spark plasma sintering (SPS). The crystallite size after densification plays an important role in improving the mechanical properties. As many researchers reported that, materials exhibiting nano-structure can improve the density, corrosion resistance, microhardness, wear resistance and compressive strength. It is very difficult to maintain nano-structure even after sintering by

conventional sintering methods like pressureless sintering due to their poor strength, poor density and obvious chance of grain growth [17]. Therefore, we have used an advanced sintering technique called as spark plasma sintering to consolidate duplex and ferritic stainless steel. By using SPS it is possible to produce nanostructured materials due to its ability to hinder grain growth and also fabricates even poorly sinterable materials during consolidation. This is due to the simultaneous application of load as well as heat on the materials to be sintered and SPS is having many advantages over conventional sintering methods [18-20]. SPS is a short time process usually takes 5 minutes, whereas conventional sintering may take few hours or even days for the same results. SPS involves discharging of spark plasma at the breaches of the particles with an 'on' and 'off' electrical current [21]. This results in the neck formation, effective thermal diffusion process between the particles, efficient shrinkage in less time, hindered grain growth and cleaner grain boundaries [1].

Keller et al. consolidated an ultra-fine grained 316L stainless steel powders using spark plasma sintering technique. They reported that, the refinement in the grain size strongly increases the hardness of the samples without much deviation from Hall-Petch relationship and concluded that, the spark plasma sintering is one of the advanced sintering technique considered as a promising tool for fabricating ultra-fine grained stainless steel [22]. S.K. Kim et al. prepared 316L stainless steel by using SPS technique at increasing temperatures from 600 to 1000°C. They observed deep dimple traces of ductile fracture at the surface of sintered body at higher sintering temperature due to the solid neck formation and its growth. They reported that, porosity of 316L stainless steel can be controlled by adding metal oxide dispersants and by controlling the punch length [23]. Lucía García et al. consolidated ball milled 316L stainless steel powder by using SPS technique. They observed tremendous decrease in the grain size from 4 µm to 350 nm after consolidating the stainless steel powders by SPS as compared to conventional sintering methods. They reported the possibility of consolidating the resulted sample with enhanced mechanical properties and retained ductility [24]. Mouawad et al. fabricated both ferritic and austenitic stainless steel by spark plasma sintering method at a temperature of 850°C. They found SPS can leads to a fully dense/nano-sized microstructure material within a short time. They reported good relationship between the Vickers hardness and the size of microstructure with the Hall-Petch equation [25]. S.R. Oke et al. studied the effect of TiN addition to spark plasma sintered duplex stainless steel samples at a sintering temperature of 1150°C. They reported that, addition of TiN to duplex stainless steel decreases the density and hardness [26]. Shashanka et al. fabricated yttria dispersed duplex and ferritic stainless steel by SPS method at a temperature of 1000°C. They studied the effect of yttria addition on the microstructure, hardness, density and wear resistant property of duplex and ferritic stainless steel. They reported that, addition of yttria can improve the mechanical properties to a great extent [1].

From the available literatures it has been found that SPS is an advanced sintering technique that can improve the mechanical properties of stainless steel by hindering the grain size. Our aim is to study the wear resistant property, density and hardness of SPS consolidated duplex and ferritic stainless steel samples. Very few literatures are available on the non-lubricated sliding wear behaviour of spark plasma sintered duplex and ferritic stainless steel. Therefore, author has taken up this challenge and reported the wear resistance, wear mechanism, shape of wear debris and volume of wear debris of duplex and ferritic stainless steel.

2. Material and Methods

The fabrication part of nano-structured duplex (Fe-18Cr-13Ni) and ferritic stainless steel (Fe-17Cr-1Ni) powder by dual drive planetary milling was reported by the authors in their previous papers [2, 8]. The crystallite size of both the stainless steel powders after 10 h of milling was found to be 9 nm. The 10 h milled duplex and ferritic stainless steel powders were consolidated by SPS (SCM 1050, Sumitomo Coal Mining Co, Ltd Japan) at a pressure of 50 MPa and 1050 °C for 5 min in a 20 mm diameter graphite die. All the consolidated stainless steel samples were polished carefully for further investigation. The microhardness and density of both the stainless steels were measured by Vickers microhardness and Archimedes methods [27, 28] respectively. Vickers microhardness studies were carried out by using LECO-LM248AT fitted with Vickers pyramidal diamond indenter. The Microstructural studies were carried out using JEOL JSM-6084LV (SEM) and Zeiss optical microscopy. The phase study of consolidated stainless steel samples were carried out in a X-ray diffraction (XRD) in a RIGAKU SmartLab using filtered Cu K α -radiation ($\lambda = 0.1542$ nm). The wear studies were carried out by using pin-on-disc wear tester (Ducom, TR-208 M1). The Rockwell diamond indenter kept at a speed of 0.0041 m/s and at 20 rpm for 15 min against duplex and ferritic stainless steel samples at room temperature with a relative humidity of 70%. All wear studies were performed at applied loads of 40 and 60 N respectively with a track radius of 2 mm. The Rockwell diamond indenter was cleaned ultrasonically and dried before and after performing the wear tests. All the tests were performed 3-4 times to obtain reproducible values. The volume of wear debris was calculated by Archard's equation [29] as follows:

$$Q = \frac{KWL}{H} \quad (1)$$

Where Q is the total volume of the wear debris produced, K is a dimensionless constant, W is the total normal load, L is the sliding distance, and H is the hardness of the softest contacting surface (original surface hardness of stainless steel). Here, the value of K was taken as 1.7×10^{-5} and 1.3×10^{-5} for ferritic and duplex stainless steels respectively [30]. The wear mechanism was studied by investigating the wear track and wear debris morphology. Figure (1) represents the schematic diagram of wear experimental set up.

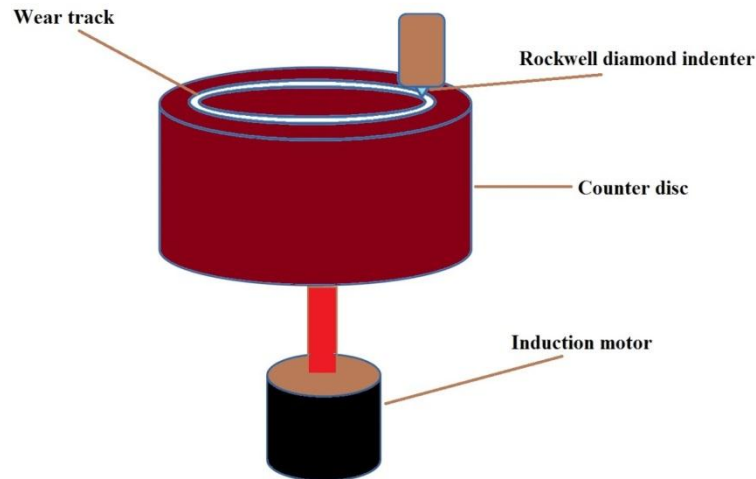


Figure 1 : The schematic diagram of wear experimental set up

3. Results and discussion

3.1 X-Ray diffraction analysis:

Figure 2 (a) and figure 2 (b) show X-ray diffraction patterns duplex and ferritic stainless steel samples consolidated by SPS at 1050°C respectively. XRD spectra of SPS consolidated duplex and ferritic stainless steel show little broad and strong crystalline diffraction peaks. The broad but yet crystalline peaks in both the stainless steel samples are due to the diffusion phenomenon as well as hindered grain growth during SPS [31]. Figure 2 (a) depicts the more dominant austenite phase due to its high temperature stability. Generally, the phase transformation of α -Fe to γ -Fe starts at a temperature of 723°C . The XRD spectra show the presence of both ferritic and austenitic phases and found no traces of diffraction peaks of secondary phases like sigma phase; carbides or nitrides precipitations. An XRD spectrum of ferritic stainless steel depicts only sharp dominant ferrite peaks as shown in the Figure 2 (b). More dominant austenite phase in duplex stainless steel is due to the reduced grain growth due to the simultaneous application of load and heat during SPS. The refinement of ferrite crystallite to nano-level can also initiate phase transformation [32].

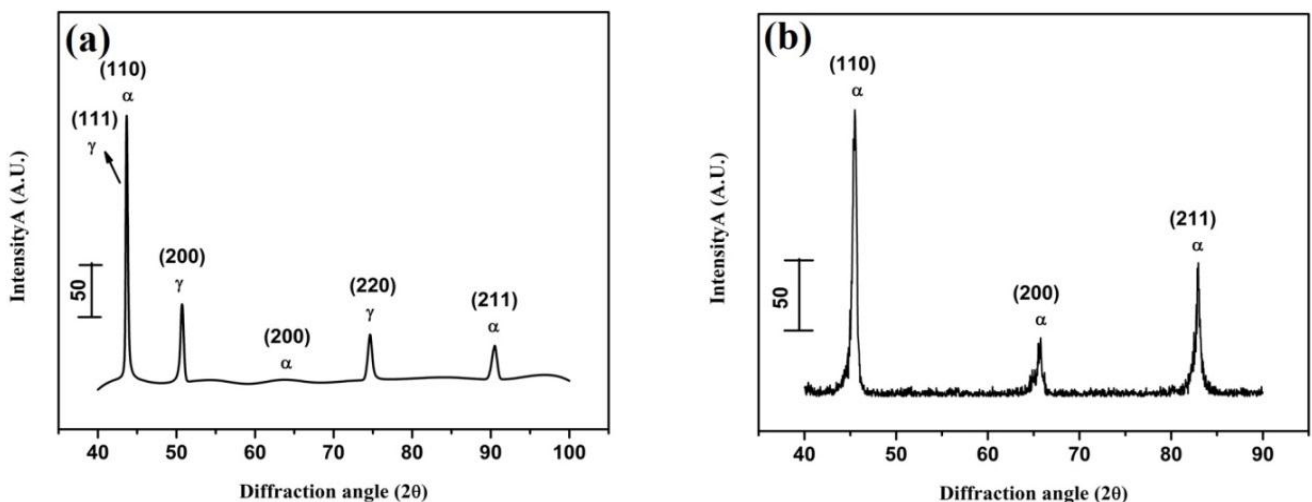


Figure 2 : XRD spectra of (a) duplex (b) ferritic stainless steel samples sintered at 1050°C by spark plasma sintering

3.2 Microstructure study:

Optical micrographs of SPS consolidated duplex and ferritic stainless steel samples are depicted in figure 3 (a) and figure 3 (b) respectively. From the figures it is clear that the consolidated stainless steel samples are dense and with low porosity ratios. This is due to rapid rate of mass transport at higher temperatures through necking and also due to the simultaneous application of load and heat. SPS duplex stainless steels exhibit acicular ferrite as shown in figure 3 (a) and they characterized by needle shaped chaotic grains of ferrite usually formed in the interior of austenite phase by nucleation on the inclusion. This chaotic order acts as obstacles for cleavage, crack propagation and hence increases the strength of stainless steel [33]. Shashanka et al also reported the formation of acicular ferrite in the SPS duplex and yttria dispersed duplex stainless steel [1]. During SPS at 1050°C, the material undergo dissolution primarily at the interior of both the stainless steel samples and part of very fine stainless steel melts and forms pendular bonds at their particle contacts [27]. The viscosity of the melted particles decreases further due to the weak and semisolid bonding between the particles. By capillary phenomenon, the low viscous liquid flows freely throughout the materials and results in rapid viscous flow sintering densification [34–36]. Therefore, both duplex and ferritic stainless steel consolidated by SPS at 1050°C exhibits low porosity ratio, high density and maximum hardness.

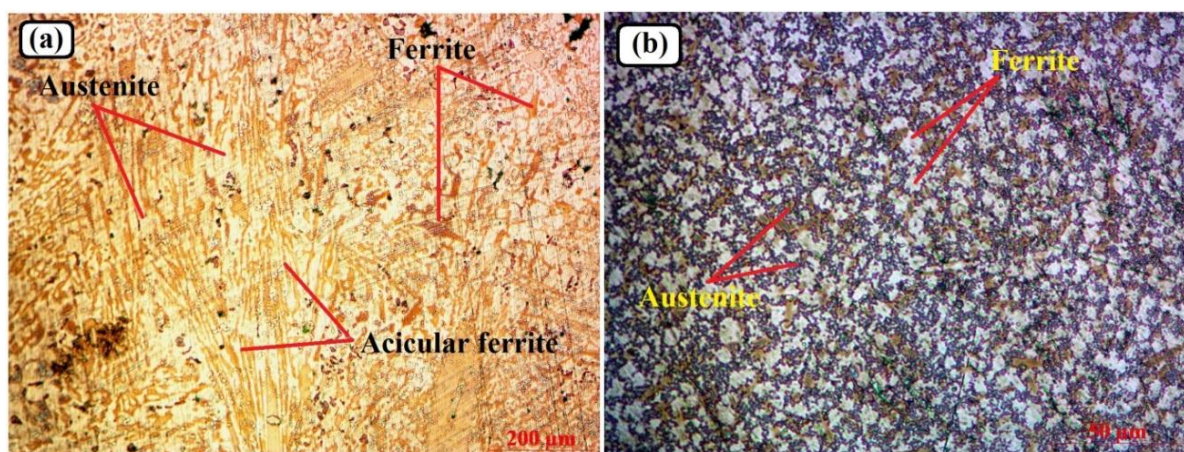


Figure 3 : Optical microstructure of (a) duplex stainless steel (b) ferritic stainless steel samples sintered at 1050°C by spark plasma sintering

3.3 Density and microhardness analysis:

Figure 4 (a) represents the density of duplex and ferritic stainless steel samples sintered by SPS method at 1050°C. The percentage density of duplex and ferritic stainless steel sintered by SPS method was found to be 94% and 96% respectively. The high density of both the stainless steel is due to the simultaneous application of load and temperature; as a result of which porosity ratio decreases to minimum value with hindered grain growth. Therefore, Spark plasma sintered stainless steel samples consists of ultrafine or nano crystalline materials [37].

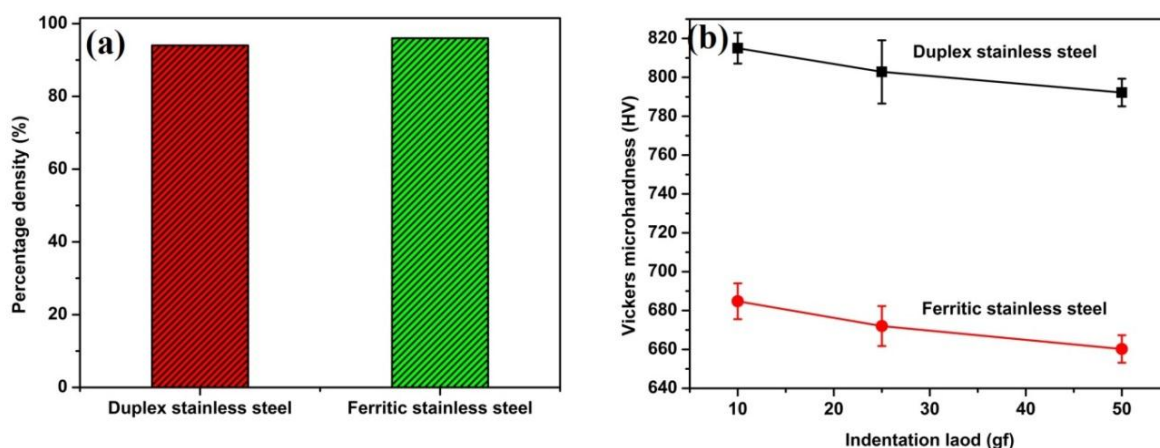


Figure 4 : Graphical representation of (a) sintered density (b) Vickers microhardness of duplex and ferritic stainless steel samples sintered at 1050°C by SPS

On the other hand figure 4 (b) represents the effect of indentation load on the microhardness of duplex and ferritic stainless steel samples spark plasma sintered at 1050°C. Indentation load of 10, 25 and 50 gf were used respectively to carry out the Vickers microhardness measurements of both the stainless steel. A minimum of 5 trials of indentations were made at each load and the average values of the diagonal lengths of indentation marks were measured as hardness for each stainless steel sample. Figure 4 (b) depicts the decrease in the Vickers microhardness value with increase in the indentation load due to indentation size effect [9, 38]. Indentation size effect is mainly due to some intrinsic structural factors such as surface dislocation pining, indentation elastic recovery and work hardening during indentation [39, 40]. Shashanka et al. reported similar kind of results in various journals [9, 27, 28]. Spark plasma sintering increases the bonding strength, density and hinders the grain growth. Duplex stainless steel show maximum hardness than ferritic stainless steels due to the decrease in the porosity ratio, increase in bonding strength, density and reduction in grain growth. The Vickers microhardness values of duplex and ferritic stainless steel sintered at 1050°C by SPS method using 25 gf indentation loads were found to be 803 HV and 672 HV respectively. Hardness and density values of duplex and ferritic stainless steel samples sintered by SPS method at 1050°C is tabulated in Table 1. The results reported in the present paper are comparable and hardness values are even higher than the results obtained by various researchers as evident in Table 1.

Table 1 : A comparison of density, hardness and sintering conditions of duplex and ferritic stainless steel consolidated by SPS by among different investigators and present research

References	Type of stainless steel	Sintering conditions	Sintering temperature (°C)	Microhardness (HV)	Sintered density (%)
[26]	TiN dispersed duplex stainless steel	SPS in vacuum, 50 MPa	1150	-	96-99%
[37]	Austenitic stainless steel	SPS in vacuum, 50 Mpa for 5 min	1000	237	99.5
[1]	Duplex stainless steel	SPS in vacuum, 50 Mpa for 5 min	1000	765	91
[1]	Ferritic stainless steel	SPS in vacuum, 50 Mpa for 5 min	1000	650	92
[41]	Yttria dispersed ferritic stainless steel	SPS, 80 Mpa load for 1 h	1050	380	97
[25]	Austenitic stainless steel	SPS, vacuum (10^{-2} mbar), 90 Mpa load	850	412	93
[42]	ODS ferritic stainless steel	SPS in Ar atmosphere, 45 MPa load for 5 min	1050	-	97
Present work	Duplex stainless steel	SPS in vacuum, 50 MPa for 5 min	1050	803	94
Present work	Ferritic stainless steel	SPS in vacuum, 50 MPa for 5 min	1050	672	96

3.4 Wear Behavior Study:

3.4.1 Effect of Load on Wear Depth:

The variation of wear depth with sliding time for duplex and ferritic stainless steel are depicted in figure 5 (a) and figure 5 (b) respectively at 40 N and 60 N applied loads. Ferritic stainless steel shows a maximum wear depth as compared to duplex stainless steel as shown in the figure 5. As SPS decreases the porosity ratio, increases the austenite phase and hinders grain growth; as result of which SPS stainless steel show lesser wear depth compared to stainless steel samples consolidated by traditional conventional methods [30]. From the figure 5, it is found that increase in applied load from 40 N to 60 N increases the wear depth in both the stainless steels. This phenomenon can be well explained by using relation [1]:

$$F = \mu N \quad (2)$$

Where, F is frictional force, N is normal load applied and μ is co-efficient of friction.

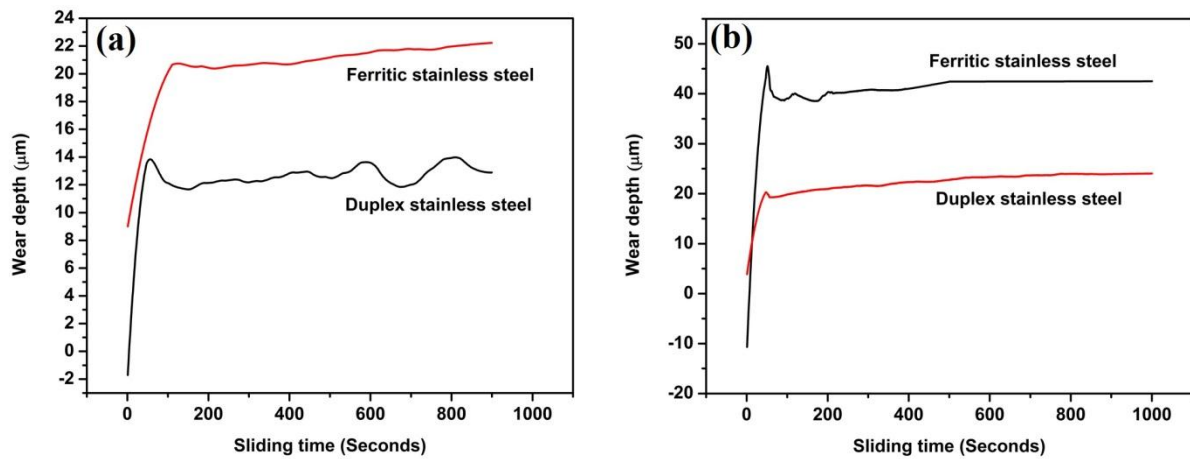


Figure 5 : Variation in wear depth of duplex and ferritic stainless steel against sliding time at a applied load of (a) 40 N (b) 60 N respectively

The Equation (2) shows that increase in normal applied load increases the frictional force. Chowdhury et al. investigated the effect of applied load (10, 15 and 20 N) on the friction co-efficient of stainless steel 304 using specially designed pin on disc wear tester at 1, 1.5 and 2 m/s sliding velocity. They reported that co-efficient of friction decreases with the increase in applied load and it increases with increase in sliding velocity [43]. Therefore, wear depth of both the stainless steel is increased with increase in applied and thereby decreasing the wear resistance as shown in the figure 5 (a) and figure 5 (b) respectively. The wear depths of duplex and ferritic stainless steels at 40 N applied load were found to be 14, 22µm, respectively. Similarly, the wear depths at 60 N applied load were found to be 23 and 41µm, respectively. As we reported, spark plasma sintered stainless steels show maximum density and hardness values; hence, the impingement of Rockwell indenter is less and therefore exhibit good wear resistant properties.

3.4.2 Wear Mechanism:

Scanning electron microscope is used to investigate the morphology of worn surface, wear mechanism, wear modes and wear debris produced by the duplex and ferritic stainless steels. Figure 6 (a) and figure 6 (b) represents the SEM images of worn surfaces of duplex and ferritic stainless steel respectively tested at 40 N applied load. It is observed from the SEM microstructure of worn surface of both the stainless steel that they undergo abrasive wear mechanism with ploughing mode. The extent of ploughing mainly depends upon the strength of the material; if the material is stronger; then ploughing impression will be mild as shown in the figure. As duplex stainless steels exhibit higher hardness values and hence undergoes mild ploughing compared to ferritic stainless steels. On the other hand, we also studied the effect of applied load on the morphology of worn surface at 60 N applied load.

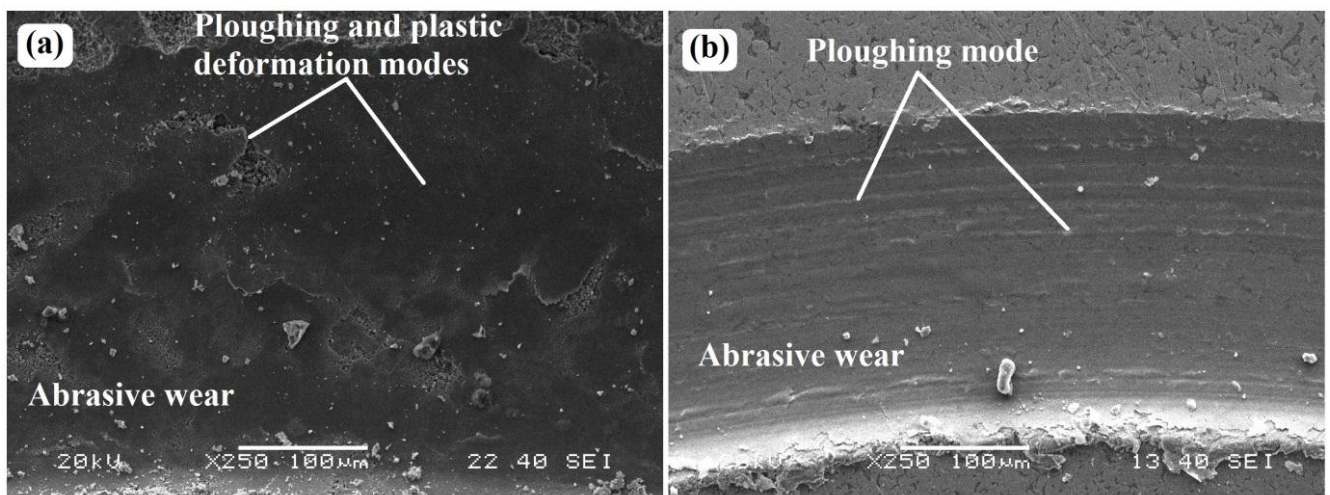


Figure 6 : Scanning electron microstructures of worn out surface of (a) duplex (b) ferritic stainless steel respectively at 40 N applied load

Figure 7 (a) and figure 7 (b) depicts the SEM images of worn surfaces of duplex and ferritic stainless steel respectively tested at 60 N applied load. From the figure 5 and figure 6, it is confirmed that the impingement of wear during 60 N applied load is more compared to wear during 40 N applied load. This enhanced material loss during 60 N applied load is due to the high frictional force. Both duplex and ferritic stainless steel samples at an applied load of 60 N exhibits abrasive and mild oxidative mechanism along with ploughing and plastic deformation modes as shown in the figure 7.

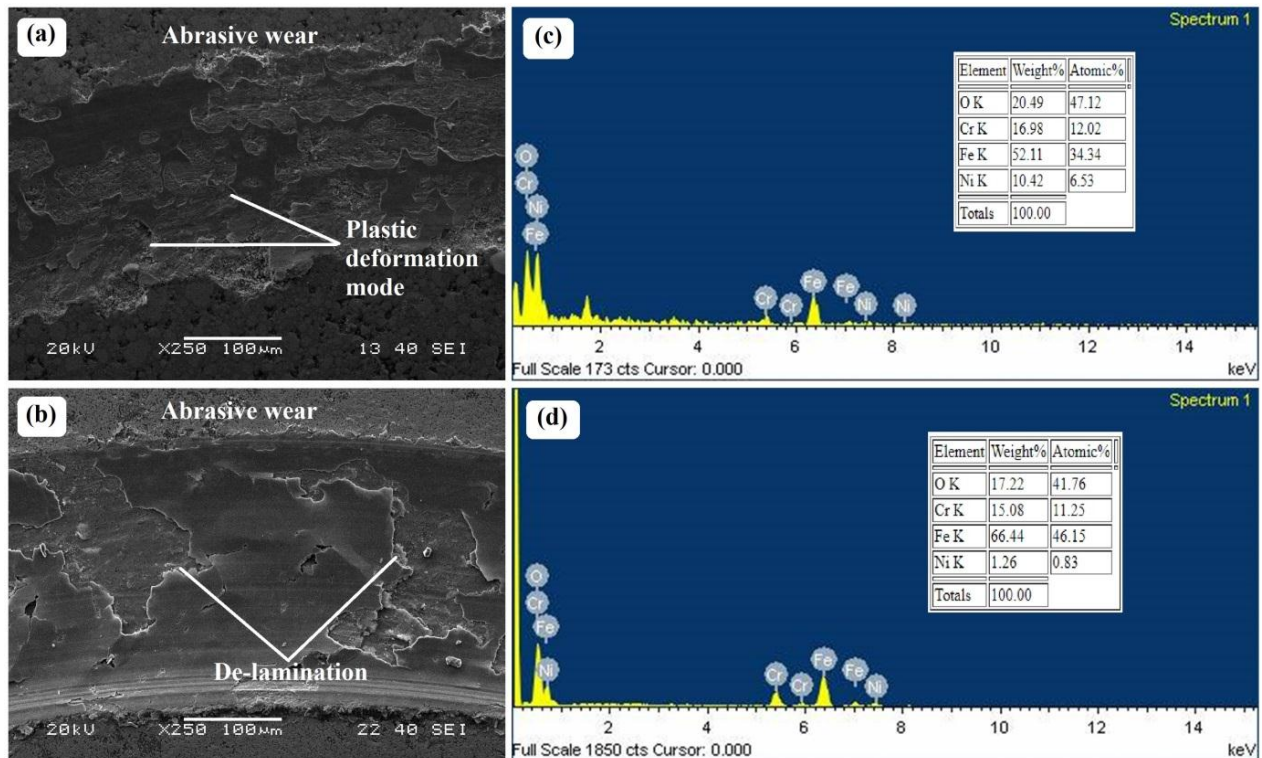


Figure 7 : SEM and EDS spectra of worn out surfaces of (a, c) duplex, (b, d) ferritic stainless steel respectively at 60 N applied load

The spark plasma sintered stainless steel shows maximum density and hardness; hence the material loss will be in the form of small powders and can easily undergo oxidation. Whereas, conventionally sintered stainless steel exhibits low density and less hardness values and hence due to the soft nature, the materials loss will be in the form of flakes [30]. The wear debris of spark plasma sintered stainless steel depicts higher surface area and surface energy due to their fine size and hence they will undergo oxidation very easily. The wear debris produced entrap in between the two contacting surfaces (stainless steel and indenter) and break the soft contacting interface (stainless steel) to a very small sizes and rapidly oxidize both wear debris and wear track surfaces [44]. Quinn [45] and Stott [46] also reported similar kind of oxidative wear mechanisms. Further investigations on oxidative mechanism are performed by using EDS to quantify the amount of oxygen present on the wear surfaces of both the stainless steel samples. Figure 7 (c) and figure 7 (d) shows the EDS spectra of worn surfaces of duplex and ferritic stainless steel at 60 N applied load. The oxygen percentage of duplex and ferritic stainless steel is found to be 20.5% and 17.2% respectively.

3.4.3 Analysis of microstructure and volume of wear debris:

Figure 8 (a) and figure 8 (b) represent the wear debris of duplex and ferritic stainless steel produced at 60 N applied load. The volume of wear debris produced at 40 N applied load is very negligible and hence wear debris were collected at 60 N applied load to study the morphology of wear mechanism. As per the microhardness study, the duplex stainless steel show higher hardness and hence it is more brittle; therefore, produced wear debris are in the form of small particles with maximum surface area. Whereas, ferritic stainless steel is soft and ductile compared to duplex stainless steel and hence produces wear debris in the form of flakes. Wear debris of duplex stainless steel are smaller in size; hence maximum surface area and more prone for oxidation than wear debris produced by ferritic stainless steel. To study the extent of wear mechanism further, we performed EDS analysis of wear debris of duplex and ferritic stainless steel at 60 N applied load and the same is depicted in the figure 8 (c) and figure 8 (d) respectively. The wear debris of duplex and ferritic stainless steel shows oxygen percentage of 26% and 24% respectively.

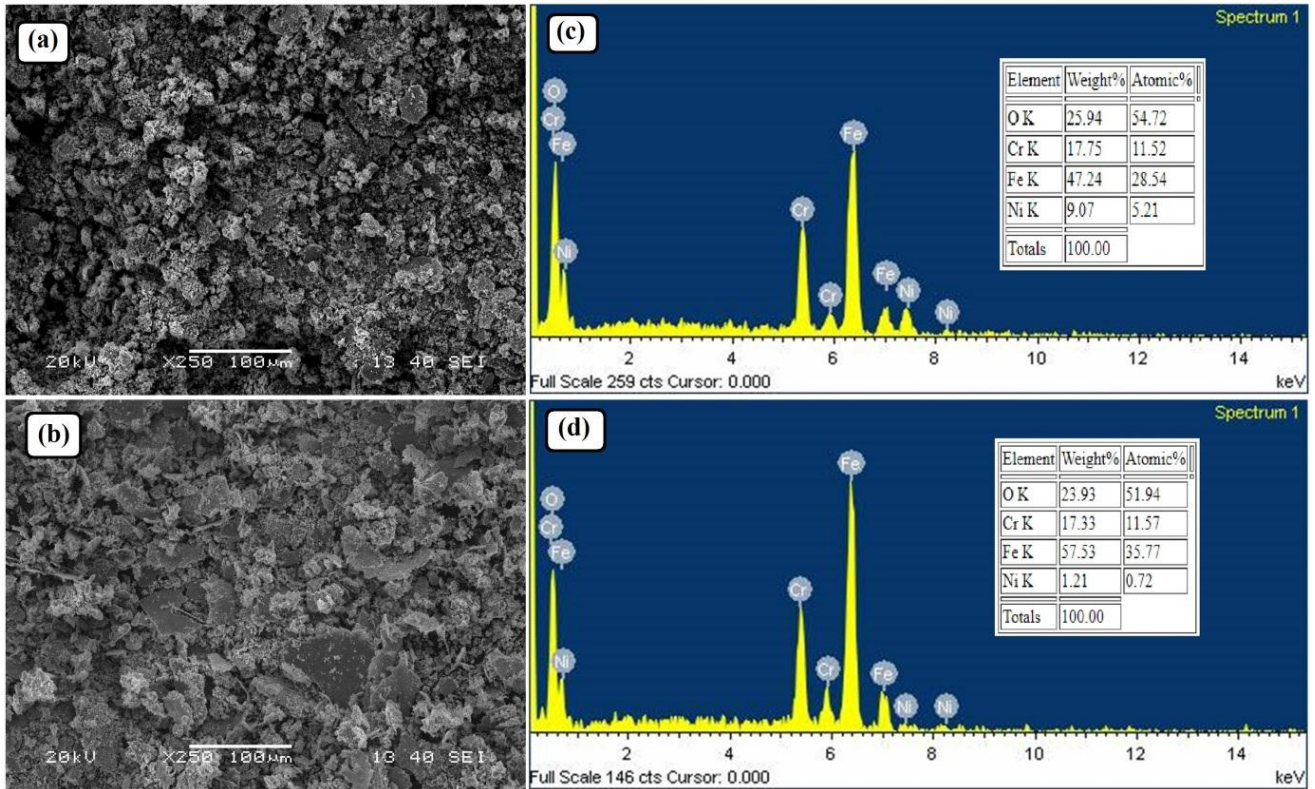


Figure 8 : SEM and EDS spectra of wear debris of (a, c) duplex, (b, d) ferritic stainless steel samples respectively at 60 N applied load

Volume of wear debris produced during wear study was calculated by Archard equation. Generally, the volume of wear debris produced mainly depends upon the hardness of materials; higher the hardness lesser will be the volume of wear debris. Figure 9 represents the volume of wear debris produced by duplex and ferritic stainless steel respectively at applied load of 40 N and 60 N. From the figure it is observed that the volume of wear debris produced increases with increase in applied load from 40 N to 60 N.

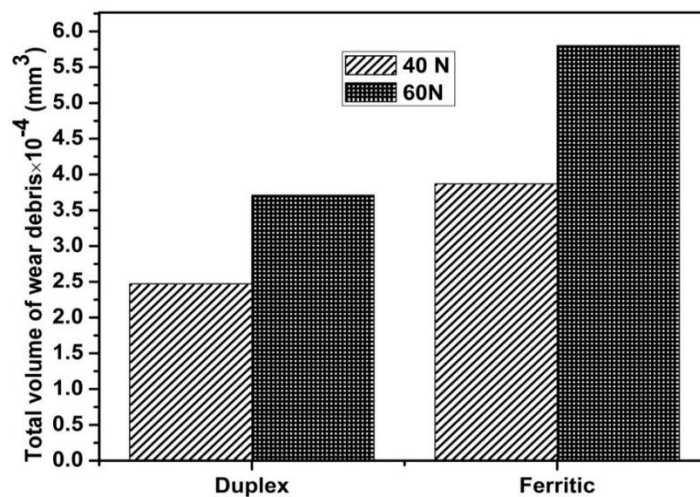


Figure 9 : The volume of wear debris produced by spark plasma sintered duplex and ferritic stainless steel at an applied load of 40 N and 60 N respectively

Wang et al. [47] and Kim et al. [48] also calculated volume of austenitic stainless steel wear debris using Archard Equation and they reported the similar kind of observation. The volume of wear debris produced by duplex and ferritic stainless steel samples at different loads are tabulated in Table 2.

Table 2 : The volume of wear debris produced by duplex and ferritic stainless steel samples at 40 N and 60 N applied loads

Type of stainless steel	Wear depth (μm)		Wear volume ($\times 10^{-4} \text{ mm}^3$)	
	40 N	60 N	40 N	60 N
Duplex stainless steel	14 \pm 8%	23 \pm 9%	2.47	3.71
Ferritic stainless steel	22 \pm 10%	41 \pm 11%	3.87	5.80

Conclusion

Planetary ball milled duplex and ferritic stainless steel powder samples were fabricated by SPS technique. We investigated the effect of spark plasma sintering on the microstructure, phase transformation, density, hardness and wear resistance of duplex and ferritic stainless steels. The percentage density of duplex and ferritic stainless steel sintered by SPS method at 1050°C is found to be 94% and 96% respectively. The Vickers microhardness values of duplex and ferritic stainless steel sintered by SPS method at 25 gf indentation load is reported to be 803 HV and 672 HV respectively. Wear depth increases with increase in applied load from 40 N to 60 N in both the stainless steels. The wear debris produced by duplex stainless steel during wear studies are in powder form. Whereas, the wear debris produced in ferritic stainless steel is flake shape and undergone de-lamination during wear due to soft nature. The wear mechanisms in duplex stainless steel are abrasive and oxidative in nature and mainly follows plastic deformation mode. On the other hand, wear mechanism of ferritic stainless steel are abrasive and oxidative but undergo de-lamination and follow ploughing mode. The amount of oxygen present on the worn surfaces of duplex and ferritic stainless steel at 60 N applied load are 20.5% and 17.2% respectively. Even wear debris of duplex stainless steel shows more oxygen percentage than wear debris of ferritic stainless steel. This confirms that, during wear duplex stainless steel is more prone for oxidation than ferritic stainless steel and this is due to the very fine wear debris of brittle materials like duplex stainless steel.

References

1. R. Shashanka, D. Chaira, D. Chakravarty, Fabrication of nano-yttria dispersed duplex and ferritic stainless steels by planetary milling followed by spark plasma sintering and non-lubricated sliding wear behaviour study. *Journal of Materials Science and Engineering B*, 6 (2016) 111-125. <https://doi.org/10.17265/2161-6221/2016.5-6.001>
2. R. Shashanka, D. Chaira, Optimization of Milling Parameters for the Synthesis of Nano-Structured Duplex and Ferritic Stainless Steel Powders by High Energy Planetary Milling, *Powder Technol.*, 278 (2015) 35-45. <https://doi.org/10.1016/j.powtec.2015.03.007>
3. R. Shashanka, D. Chaira, B.E. Kumara Swamy, Electrochemical investigation of duplex stainless steel at carbon paste electrode and its application to the detection of dopamine, ascorbic and uric acid, *International Journal of Scientific & Engineering Research*, 6 (2015) 1863–1871.
4. R. Shashanka, D. Chaira, B.E. Kumara Swamy, Fabrication of yttria dispersed duplex stainless steel electrode to determine dopamine, ascorbic and uric acid electrochemically by using cyclic voltammetry, *International Journal of Scientific & Engineering Research*, 7 (2016) 1275-1285.
5. H. Miyamoto, T. Mirnaki, S. Hashimoto, Superplastic deformation of micro-specimens of duplex stainless steel, *Mater Sci Eng A.*, 319 (2001) 779-783. [https://doi.org/10.1016/S0921-5093\(01\)01015-2](https://doi.org/10.1016/S0921-5093(01)01015-2)
6. M.J. Schofield, R. Bradsha, R.A. Cottis, Stress corrosion cracking of duplex stainless steel weldments in sour conditions, *Mater Performance*, 35 (1996) 65-70.
7. L.A. Dobrzanski, Z. Brytan, M.A. Grande, M. Rosso, Properties of duplex stainless steels made by powder metallurgy, *Arch Mater Sci Eng.*, 28 (2007) 217-23.
8. R. Shashanka, D. Chaira, Phase transformation and microstructure study of nano-structured austenitic and ferritic stainless steel powders prepared by planetary milling, *Powder Technol.*, 259 (2014) 125–136. <https://doi.org/10.1016/j.powtec.2014.03.061>
9. R. Shashanka, D. Chaira, Development of nano-structured duplex and ferritic stainless steel by pulverisette planetary milling followed by pressureless sintering, *Mater Charact.*, 99 (2015) 220-229.

10. R. Shashanka, Synthesis of nano-structured stainless steel powder by mechanical alloying-an overview, *International Journal of Scientific & Engineering Research*, 8 (2017) 588-594.
11. R. Shashanka, Investigation of Electrochemical Pitting Corrosion by Linear Sweep Voltammetry: A Fast and Robust Approach, VOLTAMMETRY, Intechopen, ISBN 978-953-51-6817-1, DOI: <http://dx.doi.org/10.5772/intechopen.80980>.
12. A.K. Nayak, R. Shashanka, D. Chaira, Effect of Nanosize Yittria and Tungsten Addition to Duplex Stainless Steel During High Energy Planetary Milling, *IOP Conf. Series: Materials Science and Engineering*, 115 (2016) 012008.
13. R. Shashanka, D. Chaira, B.E. Kumara Swamy, Electrocatalytic Response of Duplex and Yittria Dispersed Duplex Stainless Steel Modified Carbon Paste Electrode in Detecting Folic Acid Using Cyclic Voltammetry, *Int. J. Electrochem. Sci.*, 10 (2015) 5586–5598.
14. R. Shashanka, B.E. Kumara Swamy, S. Reddy, D. Chaira, Synthesis of Silver Nanoparticles and their Applications, *Anal. Bioanal. Electrochem.*, 5 (2013) 455–466.
15. S. Reddy, B.E. Kumara Swamy, S. Aruna, M. Kumar, R. Shashanka, H. Jayadevappa. Preparation of NiO/ZnO hybrid nanoparticles for electrochemical sensing of dopamine and uric acid. *Chemical Sensors*, 2 (2012) 1-7.
16. S. Gupta, R. Shashanka, D. Chaira, Synthesis of nano-structured duplex and ferritic stainless steel powders by planetary milling: An experimental and simulation study, *IOP Conf. Series: Materials Science and Engineering*, 75 (2015) 012033.
17. Ayman Elsayed, Wei Li, Omayma A. El Kady, Walid M. Daoush, Eugene A. Olevsky, Randall M. German, Experimental investigations on the synthesis of W–Cu nanocomposite through spark plasma sintering, *Journal of Alloys and Compounds*, 639 (2015) 373–380. <https://doi.org/10.1016/j.jallcom.2015.03.183>
18. M. Tokita, Trends in advanced SPS Spark Plasma Sintering systems and technology, *J. Soc. Powder Tech. Jpn.*, 30 (1993) 790-804.
19. M. Omori, Sintering, Consolidation, Reaction and Crystal Growth by the Spark Plasma System (SPS). *Mater. Sci. Eng. A.*, 287 (2000) 183-188.
20. K.H. Kim, K.B. Shim, The effect of lanthanum on the fabrication of ZrB₂–ZrC composites by spark plasma sintering. *Mater. Character.*, 50 (2003) 31-7.
21. K.H. Kim, J.H. Chae, J.S. Park, J.P. Ahn, K.B. Shim, Sintering behaviour and mechanical properties of B₄C ceramics fabricated by spark plasma sintering, *J. Ceram. Process Res.*, 10 (2009) 716-20.
22. C. Keller, K. Tabalaiev, G. Marnier, J. Noudem, X. Sauvage, E. Hug, Influence of spark plasma sintering conditions on the sintering and functional properties of an ultra-fine grained 316L stainless steel obtained from ball-milled powder, *Materials Science and Engineering A*, 665 (2016) 125–134.
23. S.K. Kim, H.T. Kim, J.S. Kim, Y.S. Kwon, Production of metal powder compact with controlled porosity by Spark plasma sintering process, Production of metal powder compact with controlled porosity by spark plasma sintering process. In Proceedings of the KORUS-2000—The 4th Korea-Russia International Symposium on Science and Technology, Ulsan, Korea, (2000) 286–290.
24. Lucía García de la Cruz, B. Flipon, C. Keller, M. Martinez, E. Hug, Nanostructuring of metals via spark plasma sintering using activated powder obtained by ball-milling: Impact on the strain-hardening mechanisms, *Proceedings of the 20th International ESAFORM Conference on Material Forming AIP Conf. Proc.*, 1896 (2017) 200002-1–200002-6; <https://doi.org/10.1063/1.5008239>.
25. B. Mouawad, D. Fabregue, M. Perez, M. Blat, F. Delabrouille, C. Domain, C. Pokor, Sintering of ferritic and austenitic nanopowders using Spark Plasma Sintering, *Metall. Res. Technol.*, 111 (2014) 305–310.
26. S.R. Oke, O.O. Ige, O.E. Falodun, B.A. Obadele, M.B. Shongwe, P.A. Olubambi, Optimization of process parameters for spark plasma sintering of nano structured SAF 2205 composite, *J. Mater. Res. Technol.*, 7 (2018) 126-134.
27. R. Shashanka, D. Chaira, Effects of Nano-Y₂O₃ and Sintering Parameters on the Fabrication of PM Duplex and Ferritic Stainless Steels, *Acta Metall. Sin. (Engl. Lett.)*, 29 (2016) 58-71.
28. R. Shashanka, Effect of Sintering Temperature on the Pitting Corrosion of Ball Milled Duplex Stainless Steel by using Linear Sweep Voltammetry, *Anal. Bioanal. Electrochem.*, 10 (2018) 349-361.

29. J.F. Archard, W. Hirst, The Wear of Metals under Unlubricated Conditions, Proceedings of the Royal Society of London A: Mathematical, Physical and Engineering Sciences, 236 (1956) 397–410.
30. R. Shashanka, D. Chaira, Effect of sintering temperature and atmosphere on non-lubricated sliding wear of nano-yttria dispersed and yttria free duplex and ferritic stainless steel fabricated by powder metallurgy, *Tribology Transactions*, 60 (2017), 324-336.
31. R. Shashanka, D. Chaira, B.E. Kumara Swamy, Effect of Y₂O₃ nanoparticles on corrosion study of spark plasma sintered duplex and ferritic stainless steel samples by linear sweep voltammetric method, *Archives of Metallurgy and Materials*, 63 (2018) 749-763.
32. Q. Meng, N. Zhou, Y. Rong, S. Chen, T.Y. Hsu, Xu Zuyao, Size effect on the Fe nanocrystalline phase transformation, *Acta Mater.*, 50 (2002) 4563–4570.
33. Bhadeshia, H.K.D. Hansraj, Honeycombe, R.W. Kerr, Steels: Microstructure and Properties (3rd ed.), Butterworth-Heinemann, (2006). ISBN 978-0-7506-8084-4.
34. R.M. German, Sintering Theory and Practice, Wiley, New York, (1996).
35. K.S. Hwang, R.M. German, F.V. Lenel, Capillary forces between spheres during agglomeration and liquid phase sintering, *Metall. Trans.*, 18A, (1987) 11-17.
36. R.M. German, Supersolidus Liquid Phase Sintering. I: Process Review, *International Journal of Powder Metallurgy*, 26 (1990) 23–34.
37. G. Marnier, C. Keller, J. Noudem, E. Hug, Functional properties of a spark plasma sintered ultrafine-grained 316L steel, *Mater. Des.*, 63 (2014) 633-40.
38. I. Manika, J. Maniks, Size effects in micro- and nanoscale indentation, *Acta Mater.*, 54 (2006) 2049-56.
39. J. Gong, J. Wu, Z. Guan, Examination of the indentation size effect in low-load Vickers hardness testing of ceramics, *J. Eur. Ceram. Soc.*, 19 (1999) 2625-2631.
40. H. Buckle, The Science of Hardness Testing and its Research Application, Edited by J.H. Westbrook, H. Conrad, Metal Park, OH, *American Society for Metals*, (1973) 453-94.
41. K.N. Allahar, J. Burns, B. Jaques, Y.Q. Wu, I. Charit, J. Cole, D.P. Butt, Ferritic oxide dispersion strengthened alloys by spark plasma sintering, *J. Nucl. Mater*, 443(2013)256-65. <https://doi.org/10.1016/j.jnucmat.2013.07.019>
42. Y.P. Xia, X.P. Wang, Z. Zhuang, Q.X. Sun, T. Zhang, Q.F. Fang, T. Hao, C.S. Liu, Microstructure and oxidation properties of 16Cr–5Al–ODS steel prepared by sol–gel and spark plasma sintering methods. *J. Nucl. Mater.*, 432 (2013) 198-204. <https://doi.org/10.1016/j.jnucmat.2012.07.039>
43. M.A. Chowdhury, D.M. Nuruzzaman, B.K. Roy, P.K. Dey, M.G. Mostafa, M.S. Islam, Md. Rashed Mia, Experimental Investigation on Friction and Wear of Stainless Steel 304 Sliding Against Different Pin Materials, *World Applied Sciences Journal*, 22(12)(2013)1702-1710. doi.org/10.5829/idosi.wasj.2013.22.12.660
44. M.C.M. Farias, R.M. Souza, A. Sinatora, D.K. Tanaka, The influence of applied load, sliding velocity and martensitic transformation on the unlubricated sliding wear of austenitic stainless steels, *Wear*, 263 (2007) 773-781. <https://doi.org/10.1016/j.wear.2006.12.017>
45. T.F.J. Quinn, Review of oxidational wear: Part I: The origins of oxidational wear. *Tribol. Int.*, 16 (1983) 257-271. [https://doi.org/10.1016/0301-679X\(83\)90086-5](https://doi.org/10.1016/0301-679X(83)90086-5)
46. F.H. Stott, The role of oxidation in the wear alloys, *Tribol. Int.*, 31 (1998) 61-71. [https://doi.org/10.1016/S0301-679X\(98\)00008-5](https://doi.org/10.1016/S0301-679X(98)00008-5)
47. B. Wang, B. Yao, Z. Han, Annealing Effect on Wear Resistance of Nanostructured 316L Stainless Steel Subjected to Dynamic Plastic Deformation, *Journal of Materials Science & Technology*, 28 (2012) 871–877. [https://doi.org/10.1016/S1005-0302\(12\)60145-5](https://doi.org/10.1016/S1005-0302(12)60145-5)
48. H. Kim, J.H. Choi, J.K. Kim, H.S. Hong, S.J. Kim, Reciprocating Sliding Wear of Inconel 600 Tubing in Room Temperature Air, *Journal of Alloys and Compounds*, 351 (2003) 309–313. [https://doi.org/10.1016/S0925-8388\(02\)01078-2](https://doi.org/10.1016/S0925-8388(02)01078-2)

(2019) ; <http://www.jmaterenvironsci.com>